Alternative erythropoietin-mediated signaling prevents secondary microvascular thrombosis and inflammation within cutaneous burns

Stefan Bohr[a,b], Suraj J. Patel[a,b], Keyue Shen[a,b], Antonia G. Vitalo[a,b], Michael Brines[c], Anthony Cerami[c], Francois Berthiaume[d], and Martin L. Yarmush[a,b,d,1]

[a]Center for Engineering in Medicine, Massachusetts General Hospital, Boston, MA 02114; [b]Shriners Hospitals for Children, Boston, MA 02114; [c]Araim Pharmaceuticals, Ossining, NY 10562; and [d]Department of Biomedical Engineering, Rutgers University, Piscataway, NJ 08854

Edited* by Charles A. Dinarello, University of Colorado Denver, Aurora, CO, and approved January 16, 2013 (received for review August 15, 2012)

Alternate erythropoietin (EPO)–mediated signaling via the heteromeric receptor composed of the EPO receptor and the β-common receptor (CD131) exerts the tissue-protective actions of EPO in various types of injuries. Herein we investigated the effects of the EPO derivative helix beta surface peptide (synonym: ARA290), which specifically triggers alternate EPO-mediated signaling, but does not bind the erythropoietic EPO receptor homodimer, on the progression of secondary tissue damage following cutaneous burns. For this purpose, a deep partial thickness cutaneous burn injury was applied on the back of mice, followed by systemic administration of vehicle or ARA290 at 1, 12, and 24 h postburn. With vehicle-only treatment, wounds exhibited secondary microvascular thrombosis within 24 h postburn, and subsequent necrosis of the surrounding tissue, thus converting to a full-thickness injury within 48 h. On the other hand, when ARA290 was systemically administered, patency of the microvasculature was maintained. Furthermore, ARA290 mitigated the innate inflammatory response, most notably tumor necrosis factor-alpha–mediated signaling. These findings correlated with long-term recovery of initially injured yet viable tissue components. In conclusion, ARA290 may be a promising therapeutic approach to prevent the conversion of partial- to full-thickness burn injuries. In a clinical setting, the decrease in burn depth and area would likely reduce the necessity for extensive surgical debridement as well as secondary wound closure by means of skin grafting. This use of ARA290 is consistent with its tissue-protective properties previously reported in other models of injury, such as myocardial infarction and hemorrhagic shock.

thermal injury | hypoxia | oxidative stress | leukocyte infiltration | cell adhesion molecules

Although the incidence of death from burns has decreased, survivors must often deal with the lifelong consequences of disfigurement and extensive scarring due to the original loss of tissue and subsequent defective healing (1–4). Burn wounds are characterized by three distinct "zones" of coagulation, stasis, and hyperemia. The zone of coagulation represents tissue that was instantly destroyed at the time of injury, which is surrounded by a zone of stasis where there is exuberant inflammation and poor perfusion (5, 6). Surrounding the zone of stasis is a zone of hyperemia where microvascular perfusion is not impaired. The zone of stasis frequently makes up a significant part of the initial wound and gradually becomes necrotic within 48 h. As a result, the initial burn expands in area and depth during this early postburn phase, thus requiring repeated surgical debridement to remove additional necrotic tissue (7, 8).

The delay in necrotic transformation of the zone of stasis provides a therapeutic window for interventions that could minimize progressive tissue damage in the burn wound. Recent studies in other types of injury have reported the existence of a local tissue-protective mechanism mediated via a ubiquitous alternative erythropoietin (EPO) signaling pathway, which is triggered by a receptor distinct from that used by erythropoesis (9). The receptor involved has relatively low affinity (nanomolar) for EPO. Therefore, physiologically relevant circulating EPO levels (picomolar) exclusively trigger the classical erythropoietic signaling pathway (10). Higher EPO levels are necessary to exert tissue protective actions and could result in an undesirable rise in hematocrit and platelets (11). In addition, the thrombocytes stimulated are highly reactive (12) and can interact with activated endothelial cells, resulting in thrombosis. Therefore, several nonerythropoietic EPO derivatives have been developed, most recently an 11 amino acid peptide known as ARA290 that mimics a portion of helix B of the EPO molecule (13, 14). ARA290 selectively binds the heteromeric receptor composed of the EPO receptor (EPO-R) and the β-common receptor (CD131), which is responsible for the tissue-protective effects of EPO and does not interact with the erythropoietic EPO-R homodimer. Because the EPO-R homodimer mediates hematopoiesis as well as platelet and endothelial cell activation, ARA290 does not affect these parameters. Herein, we investigated the impact of alternative EPO-mediated signaling on progressive tissue damage after injury in a model of deep dermal burns.

Results

First we evaluated the therapeutic effect of i.v. ARA290 administration on microvascular perfusion in burn wounds caused by a 10-s application of 90 °C water to the dorsum. For this purpose, we surgically exposed the hypodermal plane underneath the site of the scald burn and imaged the underlying deep dermal vascular network (DDVN) (Fig. 1*A*). The area occupied by the vasculature was quantified and normalized to the surrounding wound bed area at each time point. In vehicle-treated controls, relative vascular area (RVA) was assessed both at the wound center and edge, which was observed to decrease sharply very early postburn and reached a nadir by 24–48 h. In contrast, ARA290-treated groups increased RVA values by ∼10-fold in the center and ∼threefold at the edge of the wounds at the 48 h time point (Fig. 1*B*). Thus, ARA290 prevented the progressive loss of the wound bed vasculature.

To supplement morphological evidence of the microvascular preserving effect of ARA290, we investigated the gene expression of the following markers related to reperfusion stress: glutathione peroxidase 1 (GPX1), superoxide dismutase 1 (SOD1), NAD(P)H quinonic dehydrogenase 1 (Nqo1), and nuclear factor (erythroid-derived 2)-like 2 (Nfe2l2, syn.: Nrf2). Enzymes involved in protection against oxidative stress such as GPX1, SOD1, and Nqo1 were dramatically up-regulated in burn wounds at 24 h, suggesting an antioxidant response (15, 16), possibly to counterbalance reactive

Author contributions: S.B., F.B., and M.L.Y. designed research; S.B., S.J.P., K.S., and A.G.V. performed research; M.B. and A.C. contributed new reagents/analytic tools; S.B., S.J.P., K.S., and A.G.V. analyzed data; and S.B., M.B., A.C., F.B., and M.L.Y. wrote the paper.

Conflict of interest statement: M.B. and A.C. are officers of Araim Pharmaceuticals and currently hold stock in the company.

*This Direct Submission article had a prearranged editor.

[1]To whom correspondence should be addressed. E-mail: ireis@sbi.org.

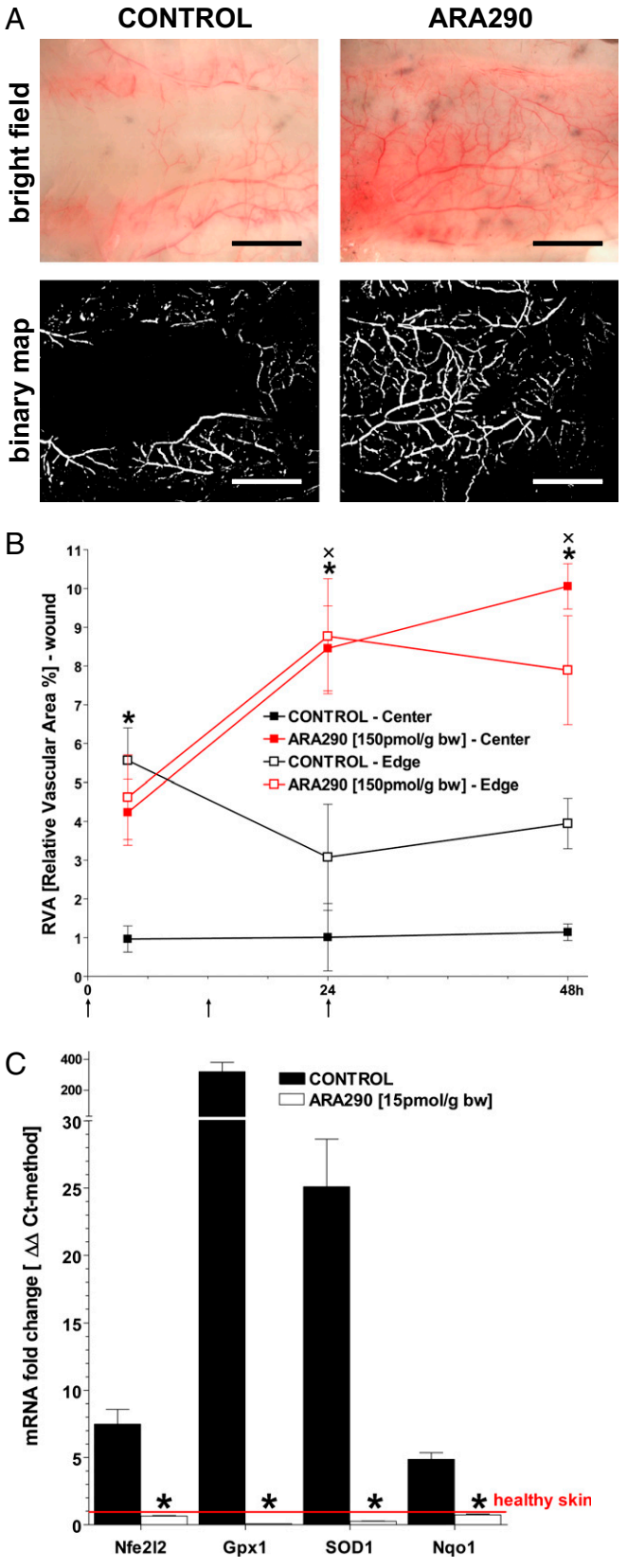

Fig. 1. ARA290 treatment salvages microvascular perfusion throughout wound beds. (*A*) The DDVN is viewed from the underside of burn wounds in controls and ARA290 (150 pmol/g bw)–treated groups, respectively. Forty-eight hours postburn, controls show a white zone of coagulation along the midline, whereas an extensive vascular network is visible in the treated group. Representative areas of the wound center and edge were analyzed for relative vessel area (RVA) (animals/time point >6). (Scale bar, 1 cm.) (*B*) RVA as a function of time ($n = 4$). ARA290 or vehicle was administered at 1, 12, and 24 h postburn as denoted by arrows along the horizontal axis (mean ± SD, *P/×$P < 0.05$ ARA290 Center/Edge vs. Control). (*C*) ARA290 inhibits burn-induced hypoxia-related mRNA levels in samples harvested 24 h postburn (qPCR/ΔΔCt-method, mean ± SD, *$P < 0.05$ vs. healthy skin).

oxidants typically released in inflammation and/or reperfusion injury (17, 18). At the gene regulatory level, Nfe2l2, a well-known inducible regulator of the antioxidant mammalian response, was also increased in control burn wounds at 24 h (Fig. 1*C*). ARA290 treatment completely suppressed these changes, thus providing biochemical evidence that ARA290 prevented tissue hypoxia.

We then evaluated the early inflammatory response in burn wounds, which is characterized by rapid infiltration by blood-borne innate immune cells, such as neutrophils and monocytes. First, we measured the total amount of cellular infiltration present based on histological nuclear staining within and around the wounds in representative tissue samples at 48 h postburn. Nuclear counts from both treated and untreated groups, as well as from the center and edge of the wounds, were plotted against the RVA measured in the same area of tissue. The wound centers of the untreated controls had low RVA that was correlated with low cellularity, and both of these parameters increased when approaching the wound edge (Fig. 2*A*). In the ARA290-treated groups, RVA was higher and similar, although cellularity increased when going from the wound center to the wound edge. Considering the entire dataset, however, there was a significant correlation of RVA vs. cellularity (Fig. 2*A*). Thus, cellular infiltration was dependent upon vascular preservation (quantified as RVA) of the wound bed, in other words accessibility through an intact/nonthrombosed microvasculature in the same tissue region. Quantification of myeloperoxidase (MPO) activity in punch biopsies retrieved from the center and edge of wounds was carried out to further assess leukocyte (mostly neutrophils and monocytes) infiltration (19). In the wound center of control animals, MPO activity peaked early, followed by a decrease to very low levels within 24 h (Fig. 2*B*), consistent with progressive thrombosis of the DDVN that prevented further access of leukocytes to the wound. After an early peak, MPO activity at the wound edge also decreased to baseline at 48 h, suggesting less thrombosis within this region. In contrast, ARA290 prevented the rapid drop in MPO activity that was seen in untreated controls, with MPO levels remaining higher during the entire course of observation, suggesting the continued presence of leukocytes in these areas. Thus, the vascular sparing effects of ARA290 allowed access of circulating leukocytes into the wound site.

Sequestered leukocytes in injured tissues are thought to be a major source of proinflammatory mediators that cause microvascular damage. Therefore, we investigated whether or not ARA290 modulates the function of leukocytes in the wounds, and more specifically the secretion of tumor necrosis factor (TNF)-α, used as a marker of leukocyte activation. The TNF-α content of tissue homogenates was measured at both the center and edge areas of the wounds and as a function of time following injury (Fig. 2 *C* and *D*). In vehicle controls, the wound center exhibited an early rise in TNF-α followed by a sharp drop at 24 h, consistent with the relatively rapid and extensive tissue necrosis in this area, whereas at the wound edge, which maintained perfusion longer, TNF-α levels peaked at 24 h and then decreased at 48 h. Conversely, wounds in the ARA290 treatment group exhibited completely different dynamics, with absence of early TNF-α spike, despite abundant cellular infiltrates, but rather a slow and progressive rise in TNF-α levels over time.

The effect of ARA290 on the inflammatory response in wounds was also assessed by measuring the transcriptional expression of several genes associated with up-regulated TNF-α

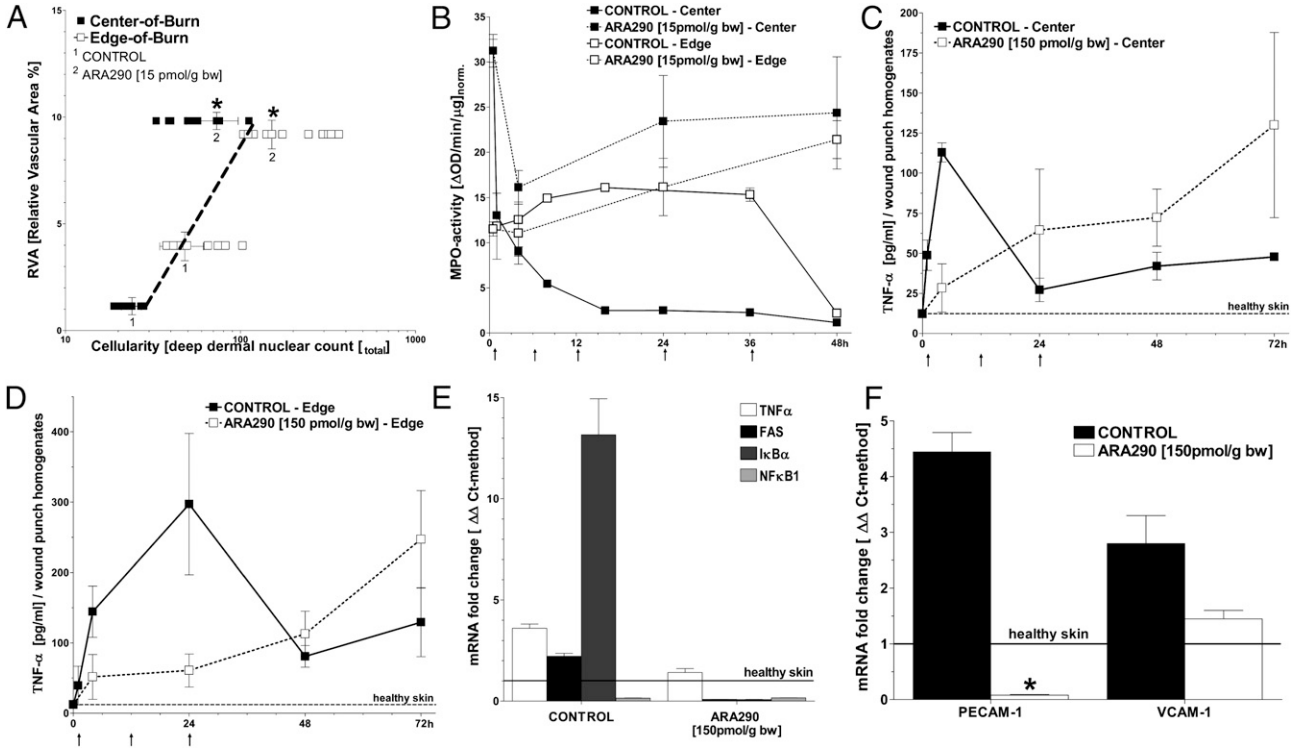

Fig. 2. ARA290 mitigates the inflammatory response in burn wounds. (*A*) Leukocyte infiltration of burn wounds with leukocytes generally correlates with RVA ($n \geq 3$, mean ± SD, $^*P < 0.05$ vs. control untreated burn wounds). (*B*) ARA290 alters the spatiotemporal dynamics of MPO activity within the wound. In central areas, MPO activity remains elevated in ARA290-treated wounds but drops ~10 fold within 16 h in controls. At the wound edge, MPO activity is slightly above initial and decreases at 48 h in controls, whereas it increases steadily over time in ARA290-treated wounds (animals/time point = 3–8). ARA290 or vehicle was given at times denoted by arrows along the horizontal axis. (*C* and *D*) In contrast, ARA290-dependent suppression of TNF-α secretion is evident in nonnecrotic wound areas that are infiltrated by leukocytes. (*E*) Results of inflammatory response profiling based on the qPCR/ΔΔCt-method show that TNF-α, FAS, and IκBα, but not NF-κB, are up-regulated in control wounds harvested 24 h postburn. This response is largely suppressed by ARA290 treatment. (*F*) Expression of adhesion molecules PECAM-1 and VCAM-1 was increased in control wounds harvested 24 h postburn vs. normal healthy skin. ARA290 suppressed PECAM-1 and to a lesser extent VCAM-1 induction. (*D* and *E*) Samples ($n = 3$, mean± SD) were normalized against normal, healthy skin; $^*P < 0.05$ vs. control untreated burn wounds.

(Fig. 2*E*). At 24 h postburn, untreated controls had significantly elevated TNF-α mRNA levels, and ARA290 treatment attenuated TNF-α induction, consistent with a decreased inflammatory response. Interestingly, expression of the pan-inflammatory marker nuclear factor kappa-light-chain-enhancer of activated B cells (NF-κB) decreased in the wound, while its inhibitory counterpart, inhibitor of NF-κB alpha (IκBα), increased by over an order of magnitude. Because NF-κB activation induces IκBα expression, it is possible that constitutively expressed NF-κB was activated in the burn wound (20), and ARA290 treatment strongly suppressed this response. It is also of interest that ARA290 mitigated the TNF-α–driven inflammatory response, as expression of the Fas receptor (FasR; synonym: CD95, TNFRS6), part of the extracellular apoptotic pathway, was also strongly suppressed.

We also investigated the effect of ARA290 on leukocyte adhesion behavior, which is an important factor of tissue infiltration and/or microvascular injury due to interactions with the vascular endothelium (21). TNF-α and interleukin (IL)-1β are known to induce cell adhesion molecules (CAMs) on the surface of the endothelium and circulating leukocytes along with other actions that cause hypercoagulability (22–24). Therefore, it is plausible that suppression of the TNF-α–driven response by ARA290 could impact on leukocyte–endothelial adhesion in the wounds. We measured gene expression of two cell CAMs, platelet endothelial CAM–1 (PECAM-1; CD31), and vascular CAM–1 (VCAM-1; CD106). Increased levels of both were found in control untreated wounds at 24h post burn compared with normal healthy skin (Fig. 2*F*). PECAM-1, although also found on endothelial cells, is predominately expressed by neutrophils and monocytes. PECAM-1 was significantly suppressed by ARA290 in the wounds to levels below that observed in normal skin.

Histologically, within 1 h postburn (Fig. 3*A*), control untreated wounds showed obvious heat-induced tissue necrosis of the epidermis and dermal hair follicles, whereas the DDVN remained largely intact with only few thrombosed vessels. At 4 h postburn,

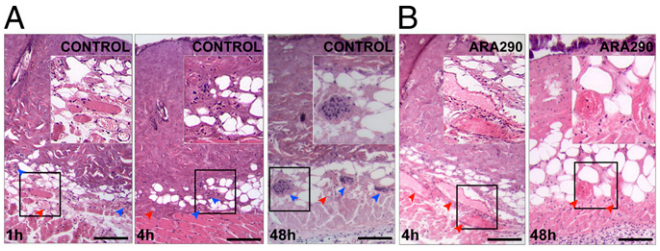

Fig. 3. ARA290 prevents progressive thrombosis of the DDVN. Areas shown are H&E stained centers of wounds. (*A*) The 1 h postburn vehicle controls exhibit patent microvessels (red arrowheads) within the deep dermis but progressive thrombosis, as evidenced by the increased number of thrombosed vessels (blue arrowheads) filled with nuclei of occluding cells, is seen at 4 h postburn. At 48 h, there is complete loss of the DDVN, as all vessels appear thrombosed. (*B*) In contrast, ARA290-treated wounds at 4 h exhibit dilated and engorged blood vessels and only few thrombosed vessels. ARA290-treated wounds maintain perfusion of the DDVN even at 48 h postburn. (Scale bar, 50 μm.) *Insets* show enlarged areas of interest.

however, there was extensive thrombosis of the DDVN, consistent with a delayed and progressive process. Of note, there was a near absence of cellular infiltrate (e.g., neutrophils) in the thrombosed areas, consistent with a lack of tissue perfusion, whereas in contrast, leukocytes accumulated in large numbers at the boundary between thrombosed and still perfused tissue. In addition to thrombosis, wound histology revealed a progressive necrosis of the hypodermal muscle layer at the later time points, ultimately leading to a full thickness skin injury. Conversely, ARA290-treated (150 pmol/g body weight i.v. at 1 h, 6 h, 12 h, 24 h, and 36 h) animals showed patent, engorged blood vessels filled with erythrocytes above the hypodermal muscle layer, and varying degrees of cellular infiltration extending all of the way into the center of the wounds (Fig. 3*B*).

To further investigate the possible effects of ARA290 treatment on immune cells in vivo, we selected a well-defined, immortalized mouse macrophage cell line (J774.A1) for use in several functional assays. First, flow cytometry performed on J774.A1 cells demonstrated >98% positive CD131 expression under standard culture conditions. We then investigated gene expression levels of the receptor alpha subunits IL-3Rα, IL-5Rα, and GM-CSF-Rα and EPO-R because they are known to dimerize with CD131, the latter acting as the intracellular beta signaling unit. TNF-α treatment of J774.A1 cells only up-regulated EPO-R and CD131 expression, whereas ARA290 suppressed this response (Fig. 4*A*). We also examined whether ARA290 modulates TNF-α expression of J774.A1 cells induced by TNF-α. ARA290 treatment alone significantly suppressed basal as well as TNF-α–mediated up-regulation of TNF-α expression (Fig. 4*B*). ARA290 also decreased PECAM-1 expression to levels below baseline in J774.A1 macrophages, and ARA290 mitigated TNF-α–driven PECAM-1 induction in these cells (Fig. 4*C*). On the other hand, ARA290 did not affect the chemotactic response of J774.A1 cells to a gradient of bacterial lipopolysaccharide (LPS) (Fig. 4*D*). Taken together, these data are consistent with alternative EPO signaling suppressing the expression of both TNF-α and PECAM-1 on macrophages.

Discussion

The major findings in this study are that (*i*) ARA290 prevents delayed microvascular thrombosis and preserves viability of deep dermal blood vessels in areas that suffered partial thickness burns, (*ii*) ARA290 mitigates TNF-α–driven responses and adhesion molecule expression in vivo and in vitro, and (*iii*) the behavior of innate immune cells that infiltrate wounds is significantly modulated by ARA290 into a less inflammatory phenotype.

The implications of these findings can be better understood by the knowledge that secondary burn wound expansion and necrosis, both in depth and width, is due to protracted tissue ischemia and inflammation. The data herein are consistent with the notion that secondary tissue damage follows the progressive thrombosis of initially patent microvasculature within burn wounds. ARA290 treatment prevented secondary thrombosis and subsequent tissue damage, but did not abolish the recruitment of leukocytes into the wounds via an intact microvascular network. Leukocyte sequestration in general is considered to promote further microvascular damage (25), and anti-inflammatory mediators that inhibit leukocyte chemotaxis, such as resolvins, have been shown to be antithrombotic in the same burn injury model (26). In vitro studies

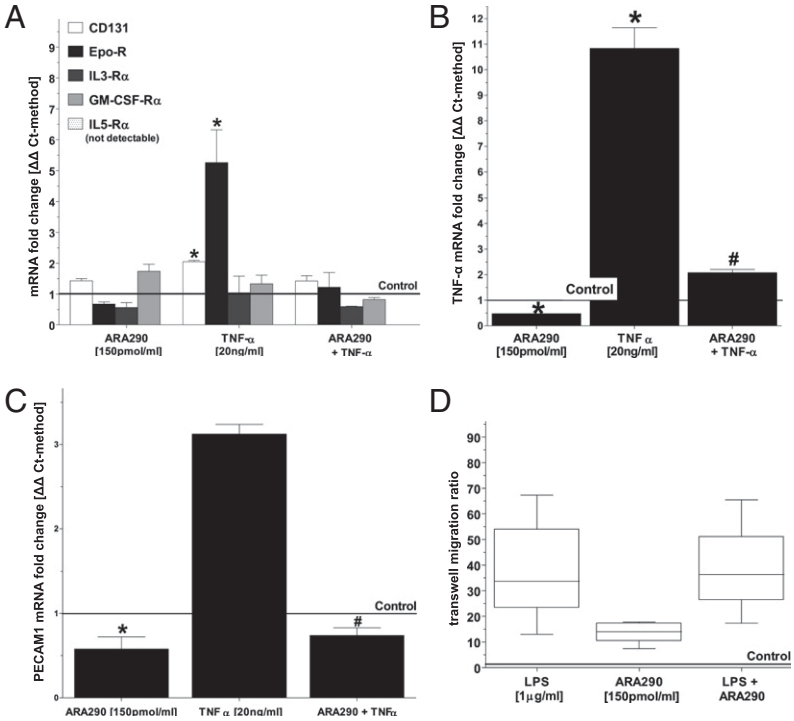

Fig. 4. ARA290 reduces TNF-α–mediated stimulation and TNF-α secretion but not chemotactic behavior of J774.A1 mouse macrophages. J774.A1 macrophages were incubated with TNF-α or vehicle for 2 h and then incubated with ARA290 or ARA297 for 6 h. The control line represents J774.A1 macrophages incubated with vehicle followed by ARA297. (*A*) Both EPO-R and CD131 are up-regulated by TNF-α, whereas other receptor subunits known to associate with CD131 remain unchanged. This induction is suppressed by ARA290 ($n \geq 3$, mean ± SD, $^{*}P < 0.05$ vs. control). (*B*) TNF-α mRNA is up-regulated by TNF-α, and suppressed by ARA290 ($n \geq 3$, mean ± SD, $^{*}P < 0.05$ vs. control, $^{\#}P < 0.05$ vs. TNF-α stimulated). (*C*) PECAM-1 mRNA is up-regulated by TNF-α. ARA290 mitigated both inducible and baseline expression of PECAM-1 ($n = 3$, mean ± SD; $^{*}P < 0.05$ vs. control, $^{\#}P < 0.05$ vs. TNF-α stimulated). (*D*) J774.A1 macrophages were added to 6 μm transwells, and migration to 1 μg/mL LPS, 150 pmol/mL ARA290, or 1 μg/mL LPS+150 pmol/mL was assessed after 3 h. Controls are J774.A1 macrophages in 150 pmol/mL ARA297. Migration in response to LPS in a transwell assay is unaffected by ARA290 ($n = 6$, box shows mean ± SEM, error bars show ± SD, $^{*}P < 0.05$ vs. controls).

on CD131-expressing J774.A1 mouse macrophages show that ARA290 alters the secretion profile of these cells, although not their chemotactic behavior. In vivo, this was most apparent by the mitigation of TNF-α secretion within burn wounds by ARA290 treatment. Thus, the preservation of microvasculature patency within burn wounds could be the result of an inhibitory effect of ARA290 on proinflammatory actions exerted by infiltrating leukocytes—for example, protection of the endothelium. It is noteworthy, although, that TNF-α levels did eventually rise above controls in the ARA290-treated group, which may reflect the fact that in these particular studies, ARA290 was not administered beyond 24 h postburn.

The data also clearly support an inhibitory effect of ARA290 on TNF-α–mediated signaling in vivo. Consistent with this notion, recent findings with ARA290 showed that it suppressed TNF-α in a urinary tract infection cell culture model (27). Other evidence of an effect on TNF-α signaling comes from studies with recombinant EPO. For example, EPO inhibited TNF-α–induced apoptosis of SH-SY5Y cells in vitro (28) as well as counteracted and reversed TNF-α–mediated effects in different in vivo models of neuronal injury (29, 30). On the other hand, EPO has also been shown to induce TNF-α and apoptosis in a liver regeneration model (31). Because the effects of EPO are not uniquely mediated via the alternative CD131/EPO-R signaling pathway, this is clear evidence for a TNF-α suppressing effect of the alternate CD131/EPO-R signaling pathway in vivo, which is selectively activated by ARA290. In a recent study, recombinant EPO was also shown to induce nitric oxide synthase at 24 h in burn wounds, which may have vasodilatory effects and contribute to improved perfusion (32); therefore, it is possible that ARA290 may exert similar effects in these experiments as well.

It is notable that previous experimental treatments of burn wounds using EPO itself have also shown tissue protection (32–35) and invoked mechanisms other than anti-inflammatory. Therefore, apart from a predominant focus on innate immunity, our findings could also be considered as only one aspect of a net effect of ARA290 on different cell types within tissues/wounds. For example, ARA290 strongly suppresses the expression of PECAM-1 and VCAM-1 in these experiments, as well as intercellular adhesion molecule 1 (ICAM-1) following shock (36), and therefore reduces the probability of thrombus formation and thereby maintains vessel patency. Also, ARA290 is known to inhibit apoptosis, including the vascular endothelial cell, within damaged tissue. Specifically it was found to increase the oxidative damage threshold for induction of the mitochondrial permeability transition in a mouse model of myocardial infarction (36). Translated to our model of burn injury, it is therefore plausible that ARA290 could increase the damage threshold needed to cause tissue death.

In conclusion, we show that systemic administration of ARA290 is highly effective in reducing burn wound expansion by preventing microvascular thrombosis and progressive necrosis, which correlated with a decrease in TNF-α secretion levels of innate immune cells, including several markers of related proinflammatory pathways in the wounds (37, 38). The decrease in burn depth and area would likely reduce the necessity for extensive surgical debridement as well as secondary wound closure by means of skin grafting. This is yet another beneficial effect of ARA290 that is consistent with prior reports of the therapeutic potential of ARA290 in other models of injury, such as myocardial infarction and hemorrhagic shock (36, 39).

Methods

Mouse Models of Burn Injury. Experiments were performed using 6-wk-old (>20 g) male C57BL/6 mice purchased from The Jackson Laboratory. To induce the burn, animals were anesthetized using i.p. ketamine+xylazine (80/6 mg/kg). The animal was positioned in a mold and the shaved back of the animal contacted with 90 °C water for 10 s, thus yielding a scald burn over 20% of the total body surface area. Untreated, this wound becomes full thickness histologically and turns into a scab, which is expelled via contraction of the wound, thus yielding a very small residual scar after several weeks. After burn, the animals received i.p. saline resuscitation (40 mL/kg/24 h) and s.c. analgesia (0.05–0.1 mg/kg buprenorphine).

Treatment. ARA290 (pyroglutamic acid-Glu-Gln-Leu-Glu-Arg-Ala-Leu-Asn-Ser-Ser-OH) was manufactured by standard F-moc solid phase peptide synthesis, purified by HPLC and ion-exchange chromatography. Unless stated otherwise, ARA290 was given via tail vein injection with 100 μL 0.9% saline as vehicle at <2 h, 12 h, and 24 h postburn. Doses used were 15 and 150 pmol/g body weight. Pilot studies were carried out using an inactive analog, ARA297, and no effects were observed compared with saline vehicle. Therefore, all studies presented herein were carried out with saline vehicle as controls.

Morphological Analysis of Wounds. Macroscopic images were taken from a standard distance using a portable digital camera (Coolpix, Nikon). Wound surface area was quantified using ImageJ 1.43u image software (http://rsbweb.nih.gov/ij/). To assess vascularity, the underside of the burn wound was surgically exposed, taking special care to avoid damaging the deep dermal vascular plane. The prepared skin was rinsed with saline, pinned to a custom-made stage, and pictures taken at 7.5× magnification using a polarizing macroscope (Olympus SZX12) mounted with a digital camera (Olympus DP10, JPN). Raw images were thresholded to highlight microvessels and analyzed using ImageJ 1.43u. RVA of the basal dermal layer was calculated as the area covered by the microvessels normalized to the total viewing area. Data shown in Fig. 1*B* were generated from six defined circular areas at the center and edge of the wounds, in at least six killed animals per time point.

Histology was performed by taking 6 mm biopsy punches from the center of the wounds. Samples were formalin fixed and paraffin embedded, cut into 5μm sections, and stained with hematoxylin and eosin (H&E).

MPO Activity Assay. Biopsy punches of 6 mm diameter were taken from the following areas: three from the wound center (>5 mm from edge of wound), three from wound edges (although entirely within the burn wound), and three from healthy skin outside of the wound (>5 mm from wound) at selected time points. At minor time points (4, 6, 8, 12, and 36 h postburn) at least three animals, and at major time points (24, 48, and 72 h postburn), at least eight animals were killed to harvest the tissues. Tissues were ground in liquid nitrogen and further processed to obtain supernatants of tissue homogenates. A modified colorimetric MPO assay was performed. In short, samples were exposed to three freeze-thaw cycles in nondenaturizing lysis buffer (20 mM Tris-HCl, 200g/L glycerol, 0.5% Tween-20) followed by three more freeze-thaw cycles and centrifugation. The MPO reaction was carried out in triplicate by first mixing 20 μL skin lysate with 20 μL assay buffer (0.167 mg/mL *o*-dianisidine-HCl, 50 mM Na_2HPO_4, pH 5.4) in a 96-well plate and, after adding 200 μL development solution (0.1% H_2O_2, 50 mM Na_2HPO_4, pH 5.4), measuring absorbance at 450 nm every 15 s. MPO activity is expressed as the change in absorbance per min per mg of skin lysate protein (ΔmOD/min/mg protein). Values for individual wounds were obtained by averaging data from the biopsies from that wound, and then data from all of the animals in each experimental group were averaged at each time point.

TNF-α ELISA. TNF-α content of tissue homogenates from defined wound areas (see above) were processed according to the manufacturer's protocol (mouse TNF-α ELISA, BD Biosciences).

Cell Culture Studies. J774.A1 mouse macrophage (catalog number TIB-67™, ATCC) cultures were maintained in standard DMEM (Dulbecco) supplemented with 200 nM L-glutamine (Sigma), 2% penicillin/streptomycin, and 10% heat-inactivated FCS. For gene expression studies, J774 macrophages were incubated with vehicle or 20 ng/mL TNF-α for 2 h. The medium was then replaced with vehicle or 150 pmol/mL ARA290, and incubated for an additional 6 h. Controls consisted of J774.A1 macrophages incubated with vehicle or 20 ng/mL TNF-α and then 150 pmol/mL ARA297. For chemotaxis assays, 2×10^5 J774.A1 macrophages were added on top of 6 μm pore-sized transwells (Millipore), and 1 μg/mL LPS, 150 pmol/mL ARA290, or 1 μg/mL LPS +150 pmol/mL ARA290 was added to the bottom well. The multiwell plate was incubated at 37 °C on an inverted microscope (Axiovert, Zeiss), and the number of cells that migrated to the bottom surface counted after 3 h of incubation. The values were then normalized to controls, which consisted of J774.A1 macrophages incubated in 150 pmol/mL ARA297.

Gene Expression Analysis. RNA was extracted from cell culture or tissue samples using either TRIzol Reagent extraction (Invitrogen) or AllPrep DNA/RNA/Protein Mini Kit (Qiagen). Total RNA quality was assessed by spectroscopy (NanoDropND-1000, ThermoScientific) and microfluidic gel analysis (Agilent RNA 6000 Nano Chip/Agilent2100 Bioanalyzer) followed by cDNA conversion using the SuperScriptIIIPlatinumTwo-StepqRT-PCR Kit (Invitrogen) or a RT^{2}FirstStand KitC-03 (SABiosciences) together with a Perkin Etus Thermal Cycler 480 (PerkinElmer). The gene expression patterns were then assessed by quantitative PCR (qPCR) with a RT^2 SYBR Green/RoxqPCR Master Mix (SABiosciences) using a Stratagene mx3005P instrument (Stratagene). A melting curve was used to confirm the specificity of each primer pair. Each sample was run in triplicate to exclude outliers. Gene expression was analyzed using the commonly used ΔΔCT method (RT^{2}qPCR Primer Assay User Manual, Version2.17, SABiosciences) with GAPDH as the normalizing gene. The average gene expression was computed for each experimental condition ($n \geq 3$) relative to the control condition ($n \geq 3$). Primers for the following genes were commercially acquired (SABiosciences): GAPDH, Gpx1, SOD1, Nqo1, Nfe2l2, and TNF-α. The following primers were designed using Primer3 v. 0.4.0 (http://frodo.wi.mit.edu/primer3/) software based on coding DNA sequences (www.ncbi.nlm.nih.gov/nuccore): CD131, forward 5′-ATGGAGGTAAAGGTCTCT-3′, reverse 5′-CTCTATAGTGAGAGGTGACA-3′; EPO-R, forward 5′-TCTGGTCCTCATCTCGCTGT-3′, reverse 5′-GCTCCACCACAGACAACCAT-3′; Fas, forward 5′-GTCAAGATTGATGAAGAAT-3′, reverse 5′-GCTGCAGACATGCTGTGGATC-3′; NFkappaB1, forward 5′-CTGACCTGAGCCTTCTGGAC-3′, reverse 5′-GCAGGCTATTGCTCATCACA-3′; mIL3-Rα, forward 5′-CCACACTACCACAGCCTTGA-3′, reverse 5′-GTCCACAGTGTTGTCCATGC-3′; mIL5-Rα, forward 5′-CAAGAGCAAAGGCATGTTGA-3′, reverse 5′-GGTGGAGCTTTGAGTTCAGC-3′; GM-CSFα, forward 5′-CACCGCGTCCTGTAACTCTT-3′, reverse 5′-GCACCTTGACCTTGTGACCT-3′; PECAM-1, forward 5′-GGAGTTTACAGAAATTATCA-3′, reverse 5′-GAAACAGCTCTGTTATGTT-3′; and VCAM-1, forward 5′-CCAGACAGACAGTCCCCTCA-3′, reverse 5′-GACCTCCACCTGGGTTCTCT-3′.

Statistics. The results are presented as mean ± SD and/or SEM. Pair wise comparisons were performed using a two-tailed Student *t* test, whereas multiple comparisons were performed by two-way analysis of variance (ANOVA) and the Bonferroni method. These analyses were performed using Prism4.0 (GraphPad) software. A two-tailed $P < 0.05$ was considered statistically significant. The number of replicates reported on the figures represents the number of wounds (equal to the number of animals) analyzed.

ACKNOWLEDGMENTS. The peptides ARA290 and ARA297 were kindly provided by Araim Pharmaceuticals, Inc. (Ossining, NY). This work was funded by the Shriners Hospital for Children. S.B. is a recipient of Deutsche Forschungsgemeinschaft (Germany) postdoctoral fellowship Award GZ: BO3468/2-1. S.J.P. was supported by a Shriners Hospital for Children postdoctoral fellowship award.

1. Lawrence JW, Mason ST, Schomer K, Klein MB (2012) Epidemiology and impact of scarring after burn injury: A systematic review of the literature. *J Burn Care Res* 33(1): 136–146.
2. Stroncek JD, Reichert WM (2008) Overview of wound healing in different tissue types. *Indwelling Neural Implants: Strategies for Contending with the in Vivo Environment*, ed Reichert WM (CRC, Boca Raton, FL).
3. Wilgus TA (2008) Immune cells in the healing skin wound: Influential players at each stage of repair. *Pharmacol Res* 58(2):112–116.
4. Schwacha MG, Thobe BM, Daniel T, Hubbard WJ (2010) Impact of thermal injury on wound infiltration and the dermal inflammatory response. *J Surg Res* 158(1):112–120.
5. Singer AJ, et al. (2010) Rapid and selective enzymatic debridement of porcine comb burns with bromelain-derived Debrase: Acute-phase preservation of noninjured tissue and zone of stasis. *J Burn Care Res* 31(2):304–309.
6. Nisanci M, Eski M, Sahin I, Ilgan S, Isik S (2010) Saving the zone of stasis in burns with activated protein C: An experimental study in rats. *Burns* 36(3):397–402.
7. Posluszny JA, Jr., Conrad P, Halerz M, Shankar R, Gamelli RL (2011) Surgical burn wound infections and their clinical implications. *J Burn Care Res* 32(2):324–333.
8. Mosier MJ, Gibran NS (2009) Surgical excision of the burn wound. *Clin Plast Surg* 36(4): 617–625.
9. Swartjes M, et al. (2011) ARA290, a peptide derived from the tertiary structure of erythropoietin, produces long-term relief of neuropathic pain: An experimental study in rats and β-common receptor knockout mice. *Anesthesiology* 115(5):1084–1092.
10. Huang X, et al. (2010) Erythropoietin receptor signaling regulates both erythropoiesis and megakaryopoiesis in vivo. *Blood Cells Mol Dis* 44(1):1–6.
11. Beguin Y (1999) Erythropoietin and platelet production. *Haematologica* 84(6): 541–547.
12. Wolf RF, et al. (1997) Erythropoietin administration increases production and reactivity of platelets in dogs. *Thromb Haemost* 78(6):1505–1509.
13. Villa P, et al. (2007) Reduced functional deficits, neuroinflammation, and secondary tissue damage after treatment of stroke by nonerythropoietic erythropoietin derivatives. *J Cereb Blood Flow Metab* 27(3):552–563.
14. Brines M, et al. (2008) Nonerythropoietic, tissue-protective peptides derived from the tertiary structure of erythropoietin. *Proc Natl Acad Sci USA* 105(31):10925–10930.
15. Boyle JJ (2005) Macrophage activation in atherosclerosis: Pathogenesis and pharmacology of plaque rupture. *Curr Vasc Pharmacol* 3(1):63–68.
16. Bernot D, Peiretti F, Canault M, Juhan-Vague I, Nalbone G (2005) Upregulation of TNF-alpha-induced ICAM-1 surface expression by adenylate cyclase-dependent pathway in human endothelial cells. *J Cell Physiol* 202(2):434–441.
17. Bischof JC, et al. (1995) Dynamics of cell membrane permeability changes at supraphysiological temperatures. *Biophys J* 68(6):2608–2614.
18. Merchant FA, Holmes WH, Capelli-Schellpfeffer M, Lee RC, Toner M (1998) Poloxamer 188 enhances functional recovery of lethally heat-shocked fibroblasts. *J Surg Res* 74(2):131–140.
19. Kothari N, et al. (2011) Increased myeloperoxidase enzyme activity in plasma is an indicator of inflammation and onset of sepsis. *J Crit Care* 26(4):435.e431–437.
20. Galkowska H, Olszewski WL, Wojewodzka U (2005) Keratinocyte and dermal vascular endothelial cell capacities remain unimpaired in the margin of chronic venous ulcer. *Arch Dermatol Res* 296(7):286–295.
21. Sese N, Cole M, Tawil B (2011) Proliferation of human keratinocytes and cocultured human keratinocytes and fibroblasts in three-dimensional fibrin constructs. *Tissue Eng Part A* 17(3-4):429–437.
22. Gillis P, et al. (1999) Keratinocyte growth factor induces angiogenesis and protects endothelial barrier function. *J Cell Sci* 112(Pt 12):2049–2057.
23. Savla U, Waters CM (1998) Barrier function of airway epithelium: Effects of radiation and protection by keratinocyte growth factor. *Radiat Res* 150(2):195–203.
24. Mak VH, et al. (1991) Barrier function of human keratinocyte cultures grown at the air-liquid interface. *J Invest Dermatol* 96(3):323–327.
25. Pober JS (1999) Immunobiology of human vascular endothelium. *Immunol Res* 19(2-3):225–232.
26. Bohr S, et al. (2013) Resolvin D2 prevents secondary thrombosis and necrosis in a mouse burn wound model. *Wound Repair Regen* 21(1):35–43.
27. Polgárová K, Lüthje P, Cerami A, Brauner A (2011) The erythropoietin analogue ARA290 modulates the innate immune response and reduces Escherichia coli invasion into urothelial cells. *FEMS Immunol Med Microbiol* 62(2):190–196.
28. Pregi N, Wenker S, Vittori D, Leirós CP, Nesse A (2009) TNF-alpha-induced apoptosis is prevented by erythropoietin treatment on SH-SY5Y cells. *Exp Cell Res* 315(3):419–431.
29. Campana WM, et al. (2006) Erythropoietin reduces Schwann cell TNF-alpha, Wallerian degeneration and pain-related behaviors after peripheral nerve injury. *Eur J Neurosci* 23(3):617–626.
30. Taoufik E, et al. (2008) TNF receptor I sensitizes neurons to erythropoietin- and VEGF-mediated neuroprotection after ischemic and excitotoxic injury. *Proc Natl Acad Sci USA* 105(16):6185–6190.
31. Klemm K, et al. (2008) Multiple doses of erythropoietin impair liver regeneration by increasing TNF-alpha, the Bax to Bcl-xL ratio and apoptotic cell death. *PLoS ONE* 3(12): e3924.
32. Tobalem M, Harder Y, Schuster T, Rezaeian F, Wettstein R (2012) Erythropoietin in the prevention of experimental burn progression. *Br J Surg* 99(9):1295–1303.
33. Galeano M, et al. (2006) Recombinant human erythropoietin improves angiogenesis and wound healing in experimental burn wounds. *Crit Care Med* 34(4):1139–1146.
34. Bader A, et al. (2012) Skin regeneration with conical and hair follicle structure of deep second-degree scalding injuries via combined expression of the EPO receptor and beta common receptor by local subcutaneous injection of nanosized rhEPO. *Int J Nanomedicine* 7:1227–1237.
35. Sorg H, Harder Y, Krueger C, Reimers K, Vogt PM (2012) The nonhematopoietic effects of erythropoietin in skin regeneration and repair: From basic research to clinical use. *Med Res Rev*, 10.1002/med.21259.
36. Patel NS, et al. (2011) A nonerythropoietic peptide that mimics the 3D structure of erythropoietin reduces organ injury/dysfunction and inflammation in experimental hemorrhagic shock. *Mol Med* 17(9-10):883–892.
37. Furse RK, Kodys K, Zhu D, Miller-Graziano CL (1997) Increased monocyte TNF-alpha message stability contributes to trauma patients' increased TNF production. *J Leukoc Biol* 62(4):524–534.
38. Segel GB, Halterman MW, Lichtman MA (2011) The paradox of the neutrophil's role in tissue injury. *J Leukoc Biol* 89(3):359–372.
39. Ahmet I, et al. (2011) A small nonerythropoietic helix B surface peptide based upon erythropoietin structure is cardioprotective against ischemic myocardial damage. *Mol Med* 17(3-4):194–200.